NATIONAL AERONAUTICS AND SPACE ADMINISTRATION

Technical Report 32-1365

Experimental and Theoretical Comparison of the JPL Active Cavity Radiometric Scale and the International Pyrheliometric Scale

Richard C. Willson

JET PROPULSION LABORATORY
CALIFORNIA INSTITUTE OF TECHNOLOGY
PASADENA, CALIFORNIA
February 1, 1969

NATIONAL AERONAUTICS AND SPACE ADMINISTRATION

Technical Report 32-1365

Experimental and Theoretical Comparison of the JPL Active Cavity Radiometric Scale and the International Pyrheliometric Scale

Richard C. Willson

JET PROPULSION LABORATORY
CALIFORNIA INSTITUTE OF TECHNOLOGY
PASADENA, CALIFORNIA
February 1, 1969

TECHNICAL REPORT 32-1365

Prepared Under Contract No. NAS 7-100
National Aeronautics and Space Administration

Preface

The work described in this report was performed by the Environmental Sciences Division of the Jet Propulsion Laboratory.

Acknowledgment

The author appreciates the invaluable assistance and advice received from James M. Kendall, Sr., Martin Berdahl, Robert E. Martin, Gordon A. Wiker, Roger M. Barnett, and Clyde L. Sydnor of JPL; the efforts of Richard B. Harris and C. L. Friswold of JPL; the contributions of Don H. Hoff, Lawrence A. Tewes, and Conrad Blankenzee of JPL who conducted the Table Mountain comparison tests; and helpful discussions with Eric G. Laue of JPL and Dr. Andrew J. Drummond of the Eppley Laboratory.

Contents

I. Introduction 1

II. Analysis of the Active Cavity Radiometer and the Accuracy of the Radiometric Scale it Defines 2

A. Principles of Operation of the Active Radiometer 2

B. Derivation of the Working Equation for the Active Cavity Radiometer 4

1. *Shutter-closed conditions* 4

2. Shutter-open conditions in the presence of an external radiation field 6

3. Shuttered measurement 6

C. Error Analysis of the Active Cavity Radiometer 7

III. Analysis of the Angstrom Pyrheliometer and the International Pyrheliometric Scale it Defines 9

A. Principles of Operation of the Angstrom Pyrheliometer 9

B. Derivation of the Working Equation for the Angstrom Pyrheliometer 10

1. Shutter closed—compensation phase 10

2. Shutter open—irradiance phase 10

3. Shuttered measurement 11

C. Error Analysis of the Angstrom Pyrheliometer 12

IV. Summary of the Error Analysis 14

V. Table Mountain Comparisons of the Active Cavity Radiometric Scale and International Pyrheliometric Scale 14

VI. Results of the Table Mountain Comparison Test 20

VII. Conclusions 22

References 23

Tables

1. Table Mountain comparison test No. 1 20

2. Table Mountain comparison test No. 2 21

Contents (contd)

Figures

1. Active Cavity Radiometer 2
2. Schematic of the electronics for the Active Cavity Radiometer 3
3. Schematic of the enclosed Active Cavity Radiometer 3
4. Active Cavity Radiometer No. 1 15
5. Major subassemblies of the enclosed Active Cavity Radiometer No. 1 16
6. Test setup for the Eppley-Angstrom Pyrheliometers Nos. 8420 and 9000 (first Table Mountain comparison test) 16
7. Active Cavity Radiometers Nos. 2 and 4 in the balloon-flight configuration 17
8. Active Cavity Radiometer instrumentation for Table Mountain test No. 2 18
9. Active Cavity Radiometer instrumentation at the Table Mountain radiometer comparison test site. 19

Abstract

The Active Cavity Radiometer, a new and accurate standard detector, has been developed for the absolute measurement of optical radiant flux. The Active Cavity Radiometric Scale, defined by the Active Cavity Radiometer, and the International Pyrheliometric Scale, defined by the Angstrom Pyrheliometer, have been compared in a recent experiment. Simultaneous measurements of solar irradiance demonstrated an average systematic difference between the two scales of 2.2% with the measurements on the Active Cavity Radiometric Scale exceeding those on the International Pyrheliometric Scale. An analytical study of the sensitivities of both the Active Cavity Radiometer and the Angstrom Pyrheliometer to common sources of experimental error is presented. The theoretical uncertainty in the Active Cavity Radiometric Scale is found to be $\pm 0.4\%$, and that of the International Pyrheliometric Scale $\pm 2.6\%$ relative to a scale based upon fundamental thermodynamic principles. Application of the average $+2.2\%$ difference between the two scales to the result of a recent extra-atmospheric solar constant measurement reported on the International Pyrheliometric Scale yields a solar constant value of $Ho = 139.1$ mW/cm^2. A recent high-altitude measurement of the solar constant and spectral distribution made by two Active Cavity radiometers yielded $Ho = 139.0$ mW/cm^2.

An Experimental and Theoretical Comparison of the JPL Active Cavity Radiometric Scale and the International Pyrheliometric Scale

I. Introduction

Scales for the measurement of radiant energy are established with respect to fundamental physical concepts by standard detectors or standard emitters of radiant energy. In some cases, both the standard detectors and emitters may be used to provide a correlation between the two methods.

Establishment of a scale of radiometry by a standard emitter usually involves the irradiance of a suitable detector by a high-temperature blackbody source of thermal radiation. If the properties of the source and the characteristics of the radiation transfer between the source and the detector are well known, the detector may be calibrated relative to the radiation scale defined by the operation of the source. The calibrated detector may then be used to measure other radiation fields and to report the results on the radiometric scale defined by its calibration. The radiant exitance of the blackbody source can be predicted very accurately from physical theory. The principal source of error in this method lies in the difficulties encountered in accurately specifying the characteristics of the propagation of source energy to the detector.

The standard detector method of defining a radiometric scale does not suffer from the propagation uncertainty. A standard detector is so designed that its interaction with an incident radiation field can be accurately predicted from a knowledge of its instrumental parameters, along with the basic framework of physical laws that defines the fundamental physics of radiation processes.

The Active Cavity Radiometric Scale is defined by the Active Cavity Radiometer, a standard detector. The Cavity Radiometer was developed at JPL (Refs. 1–3) to calibrate the vacuum radiation environments of the JPL Space Environment simulators. The original Cavity Radiometer has been enclosed in a vacuum case and modified for operation by automatic electronic circuitry. The resulting radiometric device is the Active Cavity Radiometer.

The International Pyrheliometric Scale of 1956 was defined by an International Radiation Conference held in that year. In 1957 it was adopted by the World Meteorological Organization as the international radiometric scale. It is a compromise scale, chosen as an average between the prominent radiometric scales in use at that time.

The primary instrument used to define the International Pyrheliometric Scale is the Stockholm Angstrom Pyrheliometer. In the U.S. the Eppley Laboratory of Newport, Rhode Island, maintains standard Eppley-Angstrom Pyrheliometers that are calibrated relative to the Stockholm standard. The Eppley Angstroms have been widely used as the standard of reference for radiometric measurements in the U.S.

The accuracy of a scale of radiometry relative to fundamental physical concepts can be no greater than the accuracy of the standard detector that defines the scale. Therefore, the accuracies of the Active Cavity Radiometric Scale and the International Pyrheliometric Scale can be found by an analysis of the sensitivities of the Active Cavity Radiometer and the Angstrom Pyrheliometer to common sources of experimental uncertainty.

Experimental intercomparison of the Active Cavity Radiometric Scale and the International Pyrheliometric Scale has been undertaken to make the Active Cavity Radiometric Scale available to the scientific and engineering community. Based upon the results of the comparison, any radiometric quantity or measurement previously related to the International Pyrheliometric Scale may be evaluated on the Active Cavity Radiometric Scale.

II. Analysis of the Active Cavity Radiometer and the Accuracy of the Radiometric Scale it Defines

The Active Cavity Radiometric Scale is defined by the operational principles and concepts of the Active Cavity Radiometer. To ascertain the uncertainty of measurements using this scale the sensitivity of the Active Cavity Radiometer to various sources of instrumental error will be studied. As a preface to this analysis, the basic principles of the Active Cavity Radiometer will be discussed.

A. Principles of Operation of the Active Cavity Radiometer

The Cavity Radiometer was originally developed at JPL for the calibration of radiation environments produced in space environment simulators. It has two significant advantages relative to most other standard detectors. The first and most significant advantage results from the use of a cavity detecting element. The uncertainty of the cavity aperture's absorptance for radiant flux is decreased by nearly an order of magnitude relative to that of a simple, flat detecting surface. The second major improvement over other radiometers is the precise

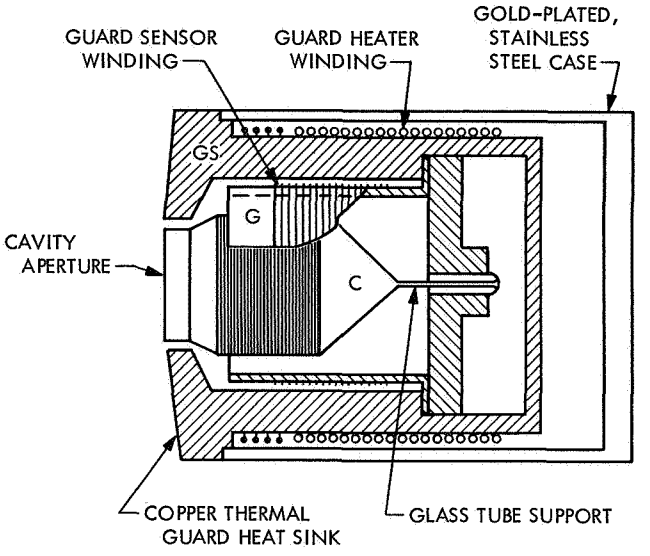

Fig. 1. Active Cavity Radiometer

thermal control, by a thermal guard, of the environment surrounding the detecting element.

The construction of the Cavity Radiometer is shown in Fig. 1. The radiometer has a low-mass, silver, cavity-detecting element (C). Its interior surface is coated with a material having a high absorptivity for the solar spectral distribution (Parsons black lacquer). Surrounding the cavity is the thermal guard (G) and heat sink (GS). Platinum resistance sensors are wound on both the cavity and the thermal guard. A guard heater is wound on the outer surface of the guard heat sink.

The cavity and guard are controlled at the same, preselected temperature by automatic, solid-state electronic circuits. Using the guard platinum winding as a sensor, the guard servo loop maintains the guard temperature by regulating the dc heating voltage applied to the guard heater winding. The cavity temperature is controlled by another servo loop which uses the cavity platinum winding as both a sensor and a heater. Figure 2 is a schematic of the operational features of the electronics.

The Active Cavity Radiometer was developed for operation in a vacuum. For operation in non-vacuum environments, the radiometer has been enclosed in a small, portable vacuum chamber. The radiometer views the source of irradiance to be measured through a quartz window. The enclosure's environmental contributions to the measured irradiance are eliminated by shuttering the irradiance on the source side of the quartz window and utilizing a differential measurement technique. Figure 3 is a schematic of the enclosed Active Cavity Radiometer.

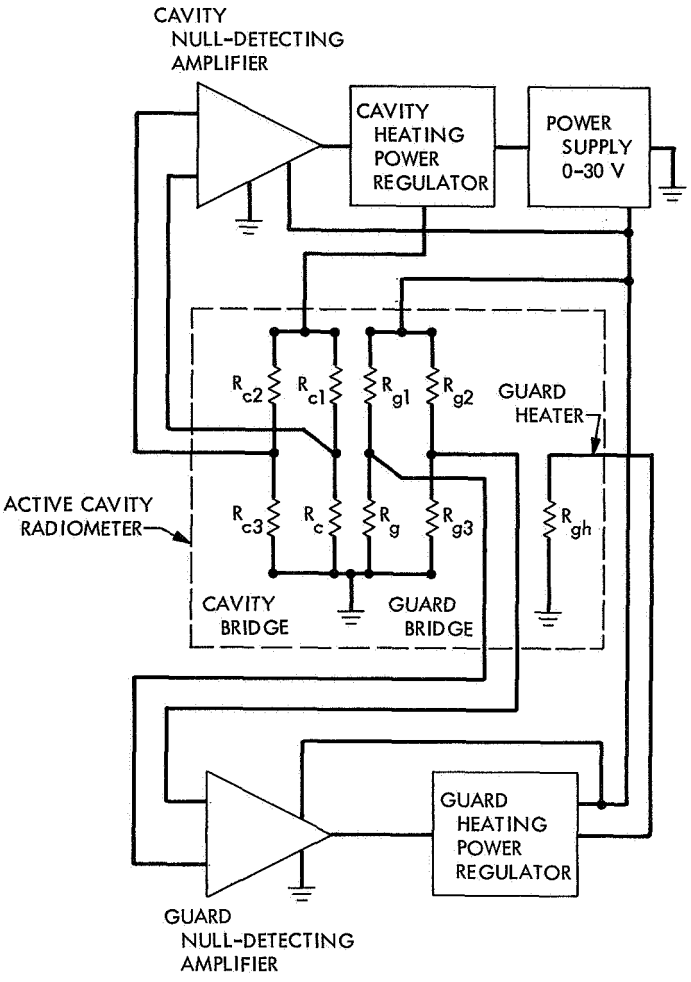

Fig. 2. Schematic of the electronics for the Active Cavity Radiometer

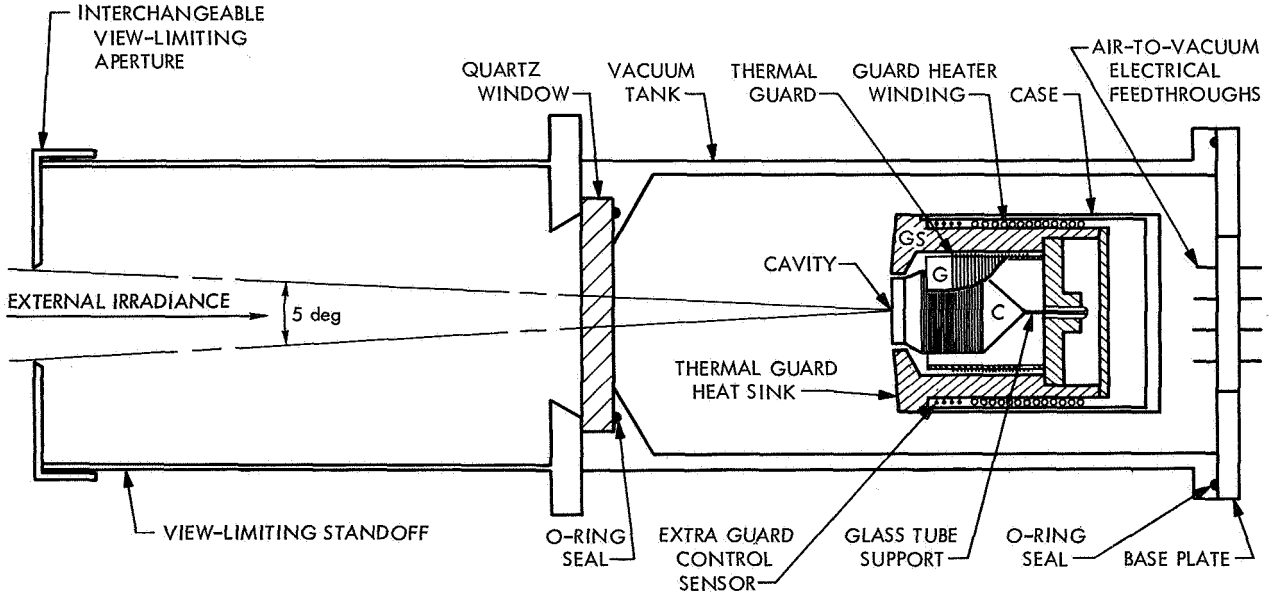

Fig. 3. Schematic of the enclosed Active Cavity Radiometer

B. Derivation of the Working Equation for the Active Cavity Radiometer

The Active Cavity Radiometer is primarily a substitution radiometer. It operates at a constant temperature and with a constant exitance at its aperture. In the absence of external irradiance, electrical heating provides the necessary power to maintain the cavity at the preselected temperature. When viewing an external source of radiation, the electrical power supplied by the servo loop decreases by an amount proportional to the irradiance of the cavity aperture. The measurement of the external radiant flux is then reduced to the measurement of the electrical power supplied to heat the cavity under the two conditions, i.e., with and without the external radiation field.

In writing the working equation for the Active Cavity Radiometer, it should first be noted that the power dissipated by the dc electrical heating of the cavity is

$$P_c = \frac{V_c^2}{R_c} \tag{1}$$

where

P_c = the cavity heating power

V_c = the voltage across the cavity sensor

R_c = the sensor's resistance

The factor $1/R_c$ will be included in a constant of proportionality K and the working equation may then be written

$$H = K\left[V_{cc}^2 - V_{co}^2\right] \tag{2}$$

where

H = the irradiance measured

K = the constant of proportionality

V_{cc} = the sensor voltage without an external radiation field

V_{co} = the sensor voltage with an external radiation field

The thermal guard principle is important in the operation of the Active Cavity Radiometer. The guard fills the 2π steradian field of view of the outside surface of the cavity. The isothermality of the cavity and guard ensures zero net radiative and conductive power transfer between them. The 2π steradian field of view of the cavity aperture does not include the thermal guard and interacts only with radiation fields external to the radiometer itself.

To demonstrate the character of the constant K in Eq. (2) the power balance of the cavity for the enclosed Active Cavity Radiometer will be analyzed. First, all the power input sources for the cavity in the absence of external radiation fields will be summed over, i.e., with the shutter closed.

1. *Shutter-closed conditions*

$$\Sigma P_{in} = P_{ec} + \rho_{IR} P_{out} + P_E + P_{cgc} \tag{3}$$

where

P_{ec} = the electrical power supplied to the cavity sensor

$\rho_{IR}P_{out}$ = the fraction of the radiant flux emitted by the radiometer and reflected back into its own aperture

P_E = the environmental infrared radiative input to the cavity aperture from the interior surface of the vacuum enclosure and the quartz window

P_{cgc} = any net radiative or conductive power input to the cavity from the guard

The interior surface of the vacuum enclosure is coated with a substance having a high, diffuse absorptance for the infrared emission spectrum of the Active Cavity Radiometer. The quartz window is also a good, long-wave, infrared absorber. The diffuse reflectivity of the enclosure walls is approximately 5%, and the specular reflectivity of the quartz window is less than 4%. Radiation transfer arguments based on these properties and the geometry show that the $\rho_{IR}P_{out}$ term is small, with $\rho_{IR} < 4 \times 10^{-4}$. P_{out} is $\cong$200 mW, which results in $\rho_{IR}P_{out} < 0.08$ mW.

The cavity and guard are maintained at the same temperature to within ± 0.1°C. The net radiative and conductive transfer between them is

$$P_{cgc} = \epsilon_g A_g \sigma T_g^4 - \epsilon_c' A_c' \sigma T_c^4 + \text{conductive inputs} \tag{4}$$

where

ϵ_g = thermal guard emittance at temperature T_g

A_g = thermal guard area seen by the outside surface of the cavity

T_g = thermal guard temperature in °K

ϵ_c = emittance of the outside cavity surface at temperature T_c

A'_c = area of the outside cavity surface

T_c = cavity temperature in °K

σ = Stefan-Boltzmann constant (5.6697×10^{-9} mW—cm^{-2}—$°K^{-4}$)

In the conductive term, the conductive heat exchange between the cavity and guard is small because of their near-isothermality. The conductive heat exchange is further reduced by utilizing slender quartz rods to support the cavity from the guard. The thermal power diffusivity of quartz is approximately 17 mW-cm^{-1}—$°C^{-1}$. There are six supportive quartz rods around the aperture and one attaching the cavity apex to the back of the thermal guard. The six aperture rods are 0.0127 cm in diameter and 0.2 cm long. The rear supporting rod is 0.1 cm in diameter and 0.5 cm long. The total heat-transfer capability for all the quartz rods is 6.5×10^{-3} mW for a 0.1°C temperature difference between the cavity and the guard. Conductive heat exchange through the 0.004-cm diameter, 2-cm long platinum leads to the cavity heater is less than 1.8×10^{-3} mW for the ±0.1°C temperature difference between the cavity and the surrounding thermal guard. These conductive heat-exchange terms are negligible relative to the 200-mW cavity operational level.

With regard to the radiative component of the P_{cgc} term, it should be noted that the mass of the guard is more than two orders of magnitude greater than the mass of the cavity. The guard's temperature will therefore vary much more slowly than the cavity's temperature so that the guard's temperature (T_g) may be taken as a constant for intervals long with respect to the time constant of the cavity. An expression may then be written for the radiative dependence of P_{cgc} on the temperature difference between the cavity and the guard by expanding P_{cgc} about the guard's temperature in a series. The first term is 0 and, by neglecting higher than first-order terms in $(T_c - T_g)$

$$P_{cgc}(T_c) = 4\,\epsilon'_c A'_c \sigma T_c^3 \delta T \qquad (T_g \text{ constant}) \tag{5}$$

where $\delta T = (T_c - T_g)$. The emittance (ϵ'_c) of the outside surface of the cavity is 0.05. The area (A'_c) of this surface is 5 cm^2. At a cavity operating temperature (T_c) of 433°K

$$P_{cgc}(T_c) < [0.5\,\text{mW/°K}]\,\delta T \tag{6}$$

For $\delta T = 0.1$°K

$$P_{cgc} < 0.05\,\text{mW} \tag{7}$$

The term P_{cgc} represents the net power transfer from the guard to the cavity when $T_g > T_c$. If $T_g < T_c$, P_{cgc} will appear with a negative sign in Eq. (3), or alternatively, with a positive sign in Eq. (9).

The $\rho_{IR}P_{out}$ and P_{cgc} terms depend only on the temperature of the cavity and the temperature difference between the cavity and guard, respectively. Since the maintenance of constant temperatures for the cavity and guard is ensured by the operational principles of the radiometer, these two terms will be the same for both phases of the shuttered measurement and will, therefore, contribute no uncertainties to the working equation. To demonstrate this, and for the sake of generality, these terms will be left in Eq. (3) for the present.

$$\Sigma P_{in} = P_{ec} + P_E + \rho_{IR} P_{out} + P_{cgc} \tag{8}$$

The sum of the power losses from the cavity with the shutter closed is

$$\Sigma P_{out} = [\epsilon_c A_c + \epsilon_a A_a]\, W_c \tag{9}$$

where

ϵ_c = the effective emittance of the cavity aperture

A_c = the cavity aperture area

ϵ_a = the effective emittance of the narrow annulus between the cavity and the guard

A_a = the area of the annulus surrounding the cavity aperture

$W_c = \sigma T_c^4$ = the black body radiant exitance

σ = the Stefan-Boltzmann constant (5.6697×10^{-9} mW/cm^2/$°K^4$)

T_c = the cavity temperature

From this, it is clear that the two terms on the right side of Eq. (9) are the radiant exitances of the cavity aperture and its surrounding annular clearance for the temperature T_c.

All measurements are made with the Active Cavity Radiometer at equilibrium, which requires that

$$\Sigma P_{in} = \Sigma P_{out} \tag{10}$$

Combining Eqs. (8) and (9)

$$P_{ec} = (\epsilon_c A_c + \epsilon_a A_a)\, W_c - P_E - [\rho_{IR} P_{out} + P_{cgc}] \tag{11}$$

2. *Shutter-open conditions in the presence of an external radiation field.* The power analysis in the shutter-open condition yields the following expression for the sum of the power inputs:

$$\Sigma P_{in} = P_{eo} + P'_E + \rho H + \tau H(\alpha_c A_c + \alpha_a A_a) + \rho_{IR} P'_{out} + P'_{cgc} \quad (12)$$

where

H = the incident irradiance on the source side of the window due to the radiation field which is to be measured

P_{eo} = the electrical heating power supplied by the servo loop to the cavity sensor

P'_E = the environmental infrared radiative input to the cavity aperture

ρH = the power input due to incident radiation reflected from the front surface of the guard to the vacuum enclosure or the quartz window, and back into the cavity aperture

τ = the effective transmittance of the quartz window for the incident spectral distribution

α_c = the effective cavity aperture absorptance for the incident spectral distribution

$\rho_{IR} P'_{out} + P'_{cgc}$ are defined as before, but apply to the shutter open phase

$\tau H\ (\alpha_c A_c + \alpha_a A_a)$ = the power input to the cavity due to the incident irradiance

The ρH term is negligibly small. Arguments similar to those previously mentioned for ρP_{out} show that the value of ρH is less than 0.05 mW.[1]

The sum of the output powers with the shutter open is obtained in the same manner as in the shutter closed condition.

$$\Sigma P_{out} = (\epsilon_c A_c + \epsilon_a A_a) W'_c \quad (13)$$

At cavity equilibrium

$$\Sigma P_{in} = \Sigma P_{out} \quad (14)$$

[1]For H = 100 mW/cm², the nominal level of solar irradiance during the Table Mountain Comparison tests.

Substituting from Eqs. (12) and (13), and by organizing terms

$$P_{eo} = (\epsilon_c A_c + \epsilon_a A_a) W'_c - P'_E - \tau H(\alpha_c A_c + \alpha_a A_a) - (\rho H + \rho_{IR} P'_{out} + P'_{cgc}) \quad (15)$$

3. *Shuttered measurement.* In one cycle of shuttered operation the powers required to maintain constant cavity aperture radiant exitance with the shutter open (P_{eo}) and with the shutter closed (P_{ec}) are measured. Subtracting Eq. (15) from Eq. (11) yields

$$P_{ec} - P_{eo} = \tau H(\alpha_c A_c + \alpha_a A_a) + [(\epsilon_c A_c + \epsilon_a A_a)(W_c - W'_c)] + [(\rho_{IR} P'_{out} + P'_{cgc}) - (\rho_{IR} P_{out} + P_{cgc})] + [P'_E - P_E] + \rho H \quad (16)$$

The constant temperature of the cavity guarantees that $W_c = W'_c$, $\rho_{IR} P_{out} = \rho_{IR} P'_{out}$, $P_{cgc} = P'_{cgc}$. If the measurement cycle is completed in a period of time that is short compared with any temperature change for the vacuum case $P_E = P'_E$, then

$$P_{ec} - P_{eo} = \tau H(\alpha_c A_c + \alpha_a A_a) + \rho H \quad (17)$$

The incident irradiance H is the quantity of interest. Neglecting the ρH term for the reasons previously explained, the following expression is obtained from Eq. (17):

$$\boxed{H = [P_{ec} - P_{eo}]\ [\tau(\alpha_c A_c + \alpha_a A_a)]^{-1}} \quad (18)$$

The electrical heating powers P_{ec} and P_{eo} are

$$P_{ec} = V_{cc}^2 R_c^{-1} \quad (19)$$

$$P_{eo} = V_{co}^2 R_c^{-1} \quad (20)$$

where

V_{cc} = the voltage across the cavity sensor with the shutter closed

V_{co} = the voltage across the cavity sensor with the shutter open

R_c = the resistance of the cavity sensor

The working equation then becomes

$$\boxed{H = [V_{cc}^2 - V_{co}^2]\ [\tau R_c (\alpha_c A_c + \alpha_a A_a)]^{-1}} \quad (21)$$

The constant of proportionality of Eq. (2) is the second term on the right hand side

$$K = [\tau R_c (\alpha_c A_c + \alpha_a A_a)]^{-1} \tag{22}$$

The term K is the calibration constant of the Active Cavity Radiometer. The specification of the parametric constituents of K facilitates the determination of irradiance (H) on the Active Cavity Radiometric Scale through the measurement of V_{cc} and V_{co}.

C. Error Analysis of the Active Cavity Radiometer

All of the instrumental parameters whose specifications facilitate the use of the Active Cavity Radiometer as a standard detector are contained in the constant K (defined in Eq. 22). The sensitivity of K to uncertainties in these parameters will first be investigated and then the uncertainties of V_{cc} and V_{co} will be included to obtain the sensitivity of the working equation to all sources of instrumental error.

The dependence of K on the instrumental parameters may be represented, in the first order of approximation, by the differential of K. Assuming no time dependences for the parametric constituents of K

$$dK = \sum_i \frac{\partial K}{\partial \xi_i} d\xi_i \tag{23}$$

where

ξ_i = the i^{th} parameter

Treating the parameters individually

$$\frac{\partial K}{\partial \tau_s} = -R_c(\alpha_{cs}A_c + \alpha_{as}A_a)\,[\tau_s R_c\,(\alpha_{cs}A_c + \alpha_{as}A_a)]^{-2} \tag{24}$$

$$\frac{\partial K}{\partial R_c} = -\tau_s\,(\alpha_{cs}A_c + \alpha_{as}A_a)\,[\tau_s R_c(\alpha_{cs}A_c + \alpha_{as}A_a)]^{-2} \tag{25}$$

$$\frac{\partial K}{\partial \alpha_{cs}} = -\tau_s R_c A_c\,[\tau_s R_c\,(\alpha_{cs}A_c + \alpha_{as}A_a)]^{-2} \tag{26}$$

$$\frac{\partial K}{\partial A_c} = -\tau_s R_c\,\alpha_{cs}\,[\tau_s R_c\,(\alpha_{cs}A_c + \alpha_{as}A_a)]^{-2} \tag{27}$$

$$\frac{\partial K}{\partial \alpha_{as}} = -\tau_s R_c\,A_a\,[\tau_s R_c\,(\alpha_{cs}A_c + \alpha_{as}A_a)]^{-2} \tag{28}$$

$$\frac{\partial K}{\partial A_a} = -\tau_s R_c\,\alpha_{as}\,[\tau_s R_c\,(\alpha_{cs}A_a + \alpha_{as}A_a)]^{-2} \tag{29}$$

where the subscript s denotes values relating to solar radiation.

Characteristic values of these parameters, along with their uncertainties, are

$\tau_s = 0.925 \pm 0.002$ (window transmittance for solar radiation)[2] (30)

$R_c = 650.0 \pm 0.5\ \Omega$ (cavity sensor resistance) (31)

$\alpha_{cs} = 0.997 \pm 0.003$ (effective cavity absorptance for solar radiation corresponding to a surface absorptance of 0.980 ± 0.020) (Refs. 4–9) (32)

[2]In general, τ_s is a function of the spectral distribution of the irradiant flux. This value was determined experimentally for the solar spectral distribution at the Table Mountain Observatory, the site of the radiometer comparison tests described in Sections V and VI.

$$A_c = 1.008 \pm 0.001 \text{ cm}^2 \qquad \text{(cavity aperture area)} \tag{33}$$

$$\alpha_{as} = 1.000 \pm 0.001 \qquad \text{(annulus absorptance for solar radiation)} \tag{34}$$

$$A_a = 0.0058 \pm 0.0006 \text{ cm}^2 \qquad \text{(annulus area)} \tag{35}$$

Computation of the contribution of each of the terms in Eqs. (24)–(29) to the total uncertainty of K may now be made using the first-order approximation for the variation of K_i

$$\delta K_i \cong \left[\frac{\partial K_a}{\partial \xi_i}\right] [\delta_{\xi_i}] \tag{36}$$

The standard deviation will be taken as the criterion for expressing the uncertainty in K. The standard deviation of K is

$$S(K) = \pm\left\{\sum_i \left[\frac{\partial K}{\partial \xi_i}\right]^2 [\delta(\xi_i)]^2\right\}^{1/2} \tag{37}$$

The parametric uncertainties stated in Eqs. (24)–(29) represent the standard deviations of measured or calculated values of the instrumental parameters. Substituting the parametric values and uncertainties into the standard deviation relationship gives for each parameter's contribution

$$\left[\frac{\partial K}{\partial \tau_s}\right]^2 [\delta \tau_s]^2 = 12.66 \times 10^{-12} \, (\text{W/cm}^{-2}/\text{V}^{-2})^2 \tag{38}$$

$$\left[\frac{\partial K}{\partial R_c}\right]^2 [\delta R_c]^2 = 1.60 \times 10^{-12} \, (\text{W/cm}^{-2}/\text{V}^{-2})^2 \tag{39}$$

$$\left[\frac{\partial K}{\partial \alpha_{cs}}\right]^2 [\partial \alpha_{cs}]^2 = 24.23 \times 10^{-12} \, (\text{W/cm}^{-2}/\text{V}^{-2})^2 \tag{40}$$

$$\left[\frac{\partial K}{\partial A_c}\right]^2 [\delta A_c]^2 = 2.63 \times 10^{-12} \, (\text{W/cm}^{-2}/\text{V}^{-2})^2 \tag{41}$$

$$\left[\frac{\partial K}{\partial \alpha_{cs}}\right]^2 [\delta \alpha_{cs}]^2 = 0.00 \times 10^{-12} \, (\text{W/cm}^{-2}/\text{V}^{-2})^2 \tag{42}$$

$$\left[\frac{\partial K}{\partial A_a}\right]^2 [\delta A_a]^2 = 0.95 \times 10^{-12} \, (\text{W/cm}^{-2}/\text{V}^{-2})^2 \tag{43}$$

From Eqs. (37)–(43), the total standard deviation of K is

$$S(K) = \pm 6.49 \times 10^{-6} \text{ W/cm}^{-2}/\text{V}^{-2} \tag{44}$$

The value of K with its standard deviation is

$$\boxed{K = 1.6455 \pm 0.0065 \text{ mW/cm}^{-2}/\text{V}^{-2}} \tag{45}$$

The error analysis is now extended to the working equation to find the net uncertainty in a measurement of solar irradiance. The working equation may be written as

$$H_s = \frac{K}{4}\left[V_c^2 - V_o^2\right] \tag{46}$$

The factor 1/4 is due to the replacement of V_{cc} and V_{co} by V_c and V_o, the cavity bridge voltages ($V_c = 2\ V_{cc}$, $V_o = 2V_{co}$).

Nominal values of the parameters V_c and V_o during the Table Mountain test were

$$V_c = 20.000 \pm 0.005\ \text{V} \tag{47}$$

$$V_o = 12.526 \pm 0.005\ \text{V} \tag{48}$$

The criterion for establishing the uncertainty in a measurement of H_s will be the standard deviation, as before. The standard deviation of measurements of H_s may be obtained by the method applied to the constant K. The ± 0.005-V uncertainties in V_c and V_o are standard deviations.

$$S(H_s) = \pm \left\{ \sum_i \left[\frac{\partial H_s}{\partial \xi_i} \right]^2 [\delta \xi_i]^2 \right\}^{1/2} \tag{49}$$

Evaluating the individual terms gives

$$\frac{\partial H_s}{\partial K} = \frac{1}{4} [V_c^2 - V_o^2] \tag{50}$$

$$\frac{\partial H_s}{\partial V_c} = \frac{K}{2} V_c \tag{51}$$

$$\frac{\partial H_s}{\partial V_o} = -\frac{K}{2} V_o \tag{52}$$

Substituting from Eqs. (45) and (47) and (48)

$$\left[\frac{\partial H_s}{\partial K} \right]^2 [\delta K]^2 = 0.156\ (\text{mW/cm}^2)^2 \tag{53}$$

$$\left[\frac{\partial H_s}{\partial V_c} \right]^2 [\delta V_c]^2 = 0.007\ (\text{mW/cm}^2)^2 \tag{54}$$

$$\left[\frac{\partial H_s}{\partial V_o} \right]^2 [\delta V_o]^2 = 0.003\ (\text{mW/cm}^2)^2 \tag{55}$$

The standard deviation of measurements of H_s made with the active cavity radiometer is

$$S(H_s) = \pm 0.41\ \text{mW/cm}^2 \tag{56}$$

The nominal value of solar irradiance measured during the Table Mountain test was 100 mW/cm². The accuracy of the measurements made by the Active Cavity Radiometer, based upon the standard deviation criterion, is ±0.41%. The uncertainty in the Active Cavity Radiometric Scale, to the nearest tenth percent, is then

$$\boxed{\pm 0.4\%} \tag{57}$$

III. Analysis of the Angstrom Pyrheliometer and the International Pyrheliometric Scale it Defines

A. Principles of Operation of the Angstrom Pyrheliometer

The Angstrom Pyrheliometer (Ref. 10) is comprised of two flat, manganin-sensing strips mounted side by side, perpendicular to the axis of, and at one end of, a metal tube. The strips are nominally 2 cm long, 0.2 cm wide, and 0.0015 cm thick. Each strip is coated on one side with a substance (usually Parson's black lacquer) having high-solar absorptance, and has a copper-constantan thermocouple attached to the other side. The 9-in.-long mounting tube is baffled to produce a 4.2- by 10.6-deg field of view for each manganin detector. A shutter mechanism allows the incident irradiance to illuminate one or both elements at a time. The tube is assumed to behave as an isothermal heat sink for one operation cycle. No active control of the tube's temperature is provided.

The standard method of operation requires balancing of the galvanometer used to monitor the outputs of the differential thermocouples with both sensor strips illuminated by the external radiation field to be measured. Then, one sensing strip is irradiated by the source (the sun for purposes of this report) and the other is heated electrically at a rate causing the two detector elements to achieve the same apparent temperature as indicated by the differential thermocouples. The roles of the two detector strips are interchanged twice, ending with the initial configuration for the final measurement of heating (compensation) current. The three measured values of heating current are averaged as four with double weight given to the second value. The irradiance is then computed by the working equation

$$H = Ci^2 \tag{58}$$

where

i = the compensation heating current

C = a constant derived from the parameters of the manganin-detecting element when the instrument is used as a true standard detector. (In practice, C is determined experimentally by

comparison with a standard International Pyrheliometric Scale instrument, the Stockholm Angstrom.)

B. Derivation of the Working Equation for the Angstrom Pyrheliometer

1. *Shutter closed—compensation phase.* In the absence of irradiance due to an external radiation field, the sum of the power inputs, per unit length, to the manganin detector during compensation is

$$\Sigma P_{in} = P_e + \alpha_{IR1}\, b\, H_{IR1} + \alpha_{IR2}\, b\, H_{IR2} + \rho_{IR} P_{out} + P_{sc} \tag{59}$$

where

P_e = the electrical heating (compensation) power per unit length of the detector

$\rho_{IR} P_{out}$ = the fraction of long wavelength infrared radiation emitted by the strip and returned by reflection per unit length of the detector

$\alpha_{IR1}\, b\, H_{IR1}, \alpha_{IR2}\, b\, H_{IR2}$ = the infrared environmental radiant power inputs to the detector, per unit length, received by the upper and lower surfaces, respectively

$\alpha_{IR1}, \alpha_{IR2}$ = the upper and lower surface absorptances for the environmental infrared radiation fields H_{IR1} and H_{IR2}. H_{IR1} and H_{IR2} represent the infrared irradiance of the detector, per unit length, due to the exitance of the tubular enclosure above and below the manganin detectors

b = the width of the manganin detecting strips (= 0.2 cm)

P_{sc} = the power input per unit length caused by the irradiance of the compensated detector by scattered radiation from a portion of sky visible to this detector through the open aperture above the other (irradiated) detector

The total power output per unit length of the detector is

$$\Sigma P_{out} = \epsilon_{IR1} W_{d_1} b + \epsilon_{IR2} W_{d_2} b + CL \tag{60}$$

where

$\epsilon_{IR1} W_{d_1} b$ = the power radiated per unit length by the upper detector surface

$\epsilon_{IR2} W_{d_2} b$ = the power radiated per unit length by the lower detector surface

CL = the power lost from the manganin detector due to conduction along leads, supports, and by convection and conduction through the air (since the Angstrom does not operate in a vacuum)

$\epsilon_{IR1}, \epsilon_{IR2}$ = the infrared emissivities of upper and lower surfaces of the detector for the spectral distribution corresponding to T_d

T_{d_i} = the detector temperature in degrees Kelvin of the upper ($i = 1$) and lower ($i = 2$) detector surfaces

$W_{d_i} = \sigma T^4_{d_i}$ the radiant exitance at temperature T_{d_i}

σ = the Stefan-Boltzmann constant

Under conditions of thermal equilibrium for the sensor strip, the following is obtained:

$$P_e = b\,[(\epsilon_{IR1} W_{d_1} + \epsilon_{IR2} W_{d_2}) - (\alpha_{IR1} H_{IR1} + \alpha_{IR2} H_{IR2})] + CL - \rho_{IR} P_{out} - P_{sc} \tag{61}$$

2. *Shutter open—irradiance phase.* With the shutter open, the upper (blackened) surface of the detector is irradiated by the external radiation field to be measured (H). The sum of the power inputs to the detector, per unit lengths, is

$$\Sigma P_{in} = \alpha b\, H + \alpha b \rho H + \alpha_{IR1}\, b\, H'_{IR1} + \alpha_{IR2}\, b\, H'_{IR2} + \rho_{IR} P'_{out} \tag{62}$$

where

αbH = the power input per unit length due to the external radiation field to be measured. For purposes of this report, this is the solar irradiance propagated through a significant fraction of the Earth's atmosphere

$\alpha b \rho H$ = the power input per unit length due to internal instrumental reflections of H

$\left.\begin{matrix} \alpha_{IR1}\, b\, H'_{IR1}, \\ \alpha_{IR2}\, b\, H'_{IR2} \end{matrix}\right\}$ = the environmental irradiant inputs per unit length

$\rho_{IR} P'_{out}$ = reflected infrared inputs for shutter open phase

H'_{IR1}, H'_{IR2} = the infrared environmental irradiances of the upper and lower detector surfaces

α = the effective absorptance of the upper detector surface for the incident, external radiation field

As in the shutter closed case, the sum of the output power is

$$\Sigma P_{out} = \epsilon_{IR1}\, b\, W'_{d_1} + \epsilon_{IR2}\, b\, W'_{d_2} + CL' \qquad (63)$$

Thermal equilibrium for the detector requires that $\Sigma P_{in} = \Sigma P_{out}$. Combining Eqs. (62) and (63) gives

$$\begin{aligned}(1 + \rho)\alpha b\, H = b\, [&(\epsilon_{IR1}\, W'_{d_1} + \epsilon_{IR2}\, W'_{d_2}) \\ &- (\alpha_{IR1}\, H'_{IR1} + \alpha_{IR2}\, H'_{IR2})] \\ &+ CL' - \rho_{IR} P'_{out}\end{aligned} \qquad (64)$$

3. *Shuttered measurement.* A cycle of measurement performed with the Angstrom Pyrheliometer may be represented mathematically by combining Eqs. (61) and (64) as follows:

$$\begin{aligned}P_e = (1 + \rho)\, \alpha b H + b\, [&\epsilon_{IR1}(W_{d_1} - W_{d'_1}) \\ &+ \epsilon_{IR2}(W_{d_2} - W_{d'_2}) \\ &+ \alpha_{IR1}\, (H'_{IR1} - H_{IR1}) + \alpha_{IR2}\, (H'_{IR2} - H_{IR2})] \\ &+ (CL - CL') + \rho_{IR}\, (P'_{out} - P_{out}) - P_{sc}\end{aligned} \qquad (65)$$

Evaluation of the right-hand side of Eq. (65) may be simplified by making certain assumptions about the parametric quantities. If the tubular enclosure does not change temperature during a cycle of measurement, $H_{IR1} = H'_{IR1}$ and $H_{IR2} = H'_{IR2}$. If the mechanisms contributing to the conduction losses CL and CL' are the same for both the shutter open and closed conditions, then $CL = CL'$. This presumes that the conductive losses of power from the irradiated and the compensated strip through their electrical leads, and the air surrounding them, are equal. This may not be the case, since the temperature distributions of the strips at apparent equilibrium, and therefore the conductive losses will, in general, be dependent upon the nature of the input power. Precise evaluation of CL and CL' would have to be performed for each Angstrom Pyrheliometer, since the instrumental design does not obviate their equivalence. A meaningful analytical treatment of this effect cannot be made; therefore, it will be assumed that $CL = CL'$, recognizing that a possible source of experimental uncertainty may be ignored. Values of the terms containing P_{out}, P'_{out}, W_{d_1}, W'_{d_1}, and W_{d_2}, W'_{d_2} depend upon the same reasoning applied to CL and CL'. Within the limits of these assumptions, $P_{out} = P'_{out}$, $W_{d_1} = W'_{d_1}$, and $W_{d_2} = W'_{d_2}$. The $\alpha b H \rho$ term can be reduced to a negligible level by proper instrument design. Using the above arguments, the first form of the Angstrom working equation is obtained from Eq. (65) as follows:

$$H = [\alpha b]^{-1}\, [P_e + P_{sc}] \qquad (66)$$

The determination of H by the measurement of P_e effectively subtracts the contribution due to P_{sc}. If P_{sc} is a significant quantity relative to H (or P_e), then the Angstrom Pyrheliometer will produce significantly lower measured values of H than an instrument without this feature. It is therefore of interest to evaluate P_{sc}.

When measuring solar radiance one of the Angstrom sensors is directly illuminated by the sun through its 4.2- × 10.6-deg aperture while the other sensor is heated electrically to produce a null for the differential thermocouple between the two. The aperture of the "compensated" sensor is blocked by a shutter that prevents its direct irradiation by the sun. However, scattered solar radiation from a region of the sky near the sun is viewed by the "compensated" sensor through the open aperture of the irradiated sensor. The P_{sc} term in Eq. (66) represents the contribution of this scattered irradiance to the power equilibrium of the compensated sensor. The magnitude of this term will depend upon the scattering characteristics of the atmosphere, the total field of view, and the proximity of the field of view to the apparent solar limb.

The sensors of the Angstrom Pyrheliometer are centered under their apertures. The rectangular field of view of one sensor, through the aperture of the other, is very nearly 4.2 × 10.6 deg. The edge of this field of view nearest to the sun is 3 deg from the apparent solar limb. This corresponds to the 4.2 deg width of the rectangular field of view extending from approximately 12 solar radii

to 28 solar radii from the center of the solar disk. At these angular distances from the sun, the order of magnitude of the ratio of scattered "sky" intensity to the solar intensity is 10^{-6} (Ref. 11). The net effect of "sky" irradiance upon the "compensated" sensor is of order 10^{-4} that due to the sun on the irradiated sensor, where a factor of 100 accounts for the relative solid angular subtendances of the sky and solar disk as seen by the sensors. As a result, the relative magnitude of the scattered and direct solar inputs are

$$P_{sc} \cong 10^{-4} P_s \tag{67}$$

where P_s represents the direct solar irradiance. Unless the scattered "sky" intensity is one to two orders of magnitude higher than that specified by Goody (Ref. 11), or an Angstrom Pyrheliometer is constructed whose "compensated" sensor views a portion of the sky much closer to the solar limb, the P_{sc} term is negligible with respect to the accuracies under discussion.

Proceeding with these assumptions, the working equation for the Angstrom Pyrheliometer is

$$H = \left[\frac{R}{\alpha b}\right] i^2 \tag{68}$$

where R = the resistance of one of the manganin sensors.

The constant of proportionality C of Eq. (58) is seen in Eq. (68) to be related to the instrumental parameters by

$$C = \frac{R}{\alpha b} \tag{69}$$

The instrumental parameters, whose specifications facilitate the use of the Angstrom Pyrheliometer as a standard detector, subject to the above assumptions, are then seen to be the resistance of the manganin sensor(s) (R), the effective absorptance of the sensor(s) for the radiation field to be measured (α), and the width of the sensor(s) (b).

In the above derivation of the working equation for the Angstrom Pyrheliometer, it was tacitly assumed that the instrumental parameters R, α, and b were the same for both sensors. The initial balancing of the galvanometer, used to monitor the differential thermocouple, will compensate the differences in α and b; however, no procedure is available for eliminating the effect of any difference in resistance between the two sensors from measurements of irradiance. A difference between the resistances of the two sensors will contribute directly to the uncertainty of measured compensation power (P_e). The instrument, for which the quantitative error analysis is presented in the next section, is the Eppley–Angstrom Pyrheliometer No. 8420, a primary U.S. standard maintained by the Eppley Laboratory of Newport, R.I. A large quantity of data was gathered by Dr. A. Drummond with this instrument during the first Table Mountain comparison test in May 1968. These data, representing the individual measurements of compensation current made in the operation of the Eppley–Angstrom Pyrheliometer No. 8420, have been analyzed for the equivalence of the two sensor strips' parameters. The compensation currents for the two strips demonstrated a systematic inequality. The currents measured for the right strip during irradiance of the left strip differed from the corresponding compensation currents measured for the left strip by an average of $+1.4\%$. During the May, 1968 comparison tests, individual determinations of both the right and left compensation currents were made during each 20-min measurement period, with the exception of period 6, in which only four individual determinations were made for each strip. The average value of the 16 current measurements was computed and used to calculate the average irradiance for the period, using the single calibration constant of the instrument. If the Angstrom No. 8420 were used as a standard detector, the 1.4% difference between its sensors would be a source of uncertainty in the determination of irradiance from the working equation derived above. Averaging of the currents from both sensors cuts in half the net effect of the 1.4% error upon the uncertainty of measured irradiance; however, in the following analysis, this source of uncertainty must be accounted for in the form of a $\pm 0.7\%$ uncertainty in the measurement of compensation currents (in addition to the instrumental limitation for measuring current of $\pm 0.1\%$).

C. Error Analysis of the Angstrom Pyrheliometer

The same type of analysis will be applied to the Angstrom Pyrheliometer that was applied to the Active Cavity Radiometer.

The composition of C of the Angstrom Pyrheliometers is shown in Eq. (69). The variation of C due to uncertainties in the values of its constituent parameters (ξ_i) may be represented by the first-order approximation

$$\delta C = \Sigma_i \frac{\partial C}{\partial \xi_i} \delta \xi_i \tag{70}$$

The individual terms are

$$\frac{\partial C}{\partial R} = [\alpha_s b]^{-1} \tag{71}$$

$$\frac{\partial C}{\partial \alpha_s} = -Rb\,[\alpha_s b]^{-2} \tag{72}$$

$$\frac{\partial C}{\partial b} = -R\,\alpha_s\,[\alpha_s b]^{-2} \tag{73}$$

The Eppley-Angstrom Pyrheliometer No. 8420 used in the Table Mountain test had the following values for these parameters:

$$\begin{cases} C = 6.920\ \text{cal/cm}^{-2}/\text{min}^{-1}/\text{A}^{-2}\ \text{(footnote}^3\text{)} \\ C = 0.4828\ \text{W/cm}^{-2}/\text{A}^{-2} \end{cases} \tag{74}$$

$$\alpha_s = 0.980 \pm 0.020\ \text{(Refs. 8, 9, and 10)}^3 \tag{75}$$

(the same uncertainty of surface properties was assumed for the Active Cavity Radiometer. α_s is the absorptance for solar radiation)

$$^4R = 0.0946 \pm 9.46 \times 10^{-5}\ \Omega(\pm 0.1\%) \tag{76}$$

$$b = 0.200 \pm 2.00 \times 10^{-4}\ \text{cm}\ (\pm 0.1\%)\ \text{(Ref. 10)} \tag{77}$$

The standard deviation will again, as with the Active Cavity Radiometer, be the criterion for establishing the uncertainty in C. The standard deviation of C is

$$S(C) = \pm \left\{ \sum_i \left[\frac{\partial C}{\partial \xi i}\right]^2 [S(\xi_i)]^2 \right\}^{1/2} \tag{78}$$

If the uncertainties in the measured or calculated values of the parameters of Eq. (77) are taken as their standard deviations, the following are obtained by evaluating the individual terms:

$$\left[\frac{\partial C}{\partial R}\right]^2 [\delta R]^2 = 0.233 \times 10^{-6}\ (\text{W/cm}^{-2}/\text{A}^{-2})^2 \tag{79}$$

$$\left[\frac{\partial C}{\partial \alpha_s}\right]^2 [\delta \alpha_s]^2 = 97.02 \times 10^{-6}\ (\text{W/cm}^{-2}/\text{A}^{-2})^2 \tag{80}$$

$$\left[\frac{\partial C}{\partial b}\right]^2 [\delta b]^2 = 0.233 \times 10^{-6}\ (\text{W/cm}^{-2}/\text{A}^{-2})^2 \tag{81}$$

[3]Data supplied to JPL by Drummond, A., the Eppley Laboratory, Inc., Newport, Rhode Island, May 15, 1968.

[4]The value of R is derived from Eq. (69) using the specification of C, α_s, and b supplied by the Eppley Laboratory.

The standard deviation of the constant C is

$$S(C) = \pm 9.9 \times 10^{-3}\ \text{W/cm}^{-2}/\text{A}^{-2} \tag{82}$$

The calibration constant, along with its uncertainty is

$$\boxed{C = 482.8 \pm 9.9\ \text{mW/cm}^{-2}/\text{A}^{-2}} \tag{83}$$

Extending the same principles to the working equation, the following relationship is obtained for the variation of irradiance:

$$\delta H_s = \sum_i \frac{\partial H_s}{\partial \xi_i}\,\delta \xi_i \tag{84}$$

During actual measurements with the Angstrom, only one fourth of the compensation current was measured so that the working equation becomes

$$H_s = 16\,Ci_m^2 \quad (i_m = i/4) \tag{85}$$

The individual terms of Eq. (84) are then

$$\frac{\partial H_s}{\partial i_m} = 32\,Ci_m \tag{86}$$

$$\frac{\partial H_s}{\partial C} = 16\,i_m^2 \tag{87}$$

A nominal value of i_m for the Table Mountain test was 0.1138 ± 0.0009 A (i.e., $[\pm(0.7\% + 0.1\%)]$)[5] (corresponding to approximately 100 mW/cm^2 irradiance). Using this figure, and the values for C in Eq. (83) the contributions of the individual terms can be computed to the total uncertainty in a measurement of solar irradiance at the 100 mW/cm^2 level.

The standard deviation of H_s may be determined as before

$$S(H_s) = \pm \left\{ \sum_i \left[\frac{\partial H_s}{\partial \xi_i}\right]^2 [S(\xi_i)]^2 \right\}^{1/2} \tag{88}$$

and, evaluating individual terms

$$\left[\frac{\partial H_s}{\partial i_m}\right]^2 [\delta i_m]^2 = 2.504\ (\text{mW/cm}^{-2})^2 \tag{89}$$

$$\left[\frac{\partial H_s}{\partial C}\right]^2 [\delta C]^2 = 4.208\ (\text{mW/cm}^{-2})^2 \tag{90}$$

[5]See Section III-B-3, last paragraph.

The resulting standard deviation of measurements of H_s made at the 100 mW/cm² level can then be calculated from Eq. (88) as follows:

$$S(H_s) = \pm 2.59 \text{ mW/cm}^{-2} \tag{91}$$

At the nominal 100 mW/cm² level of solar irradiance observed during the Table Mountain comparison tests, the measurements made by the Eppley-Angstrom Pyrheliometers were uncertain by[6]

$$\boxed{\delta H_s = \pm 2.6\%} \tag{92}$$

IV. Summary of the Error Analyses

The principal source of error for both the Active Cavity Radiometer and the Angstrom Pyrheliometer is the ±2% uncertainty assumed for the surface absorptance of their detecting elements. In the case of the Active Cavity Radiometer, the cavity geometry reduces the net cavity absorptance uncertainty from ±2% to ±0.3% (Refs. 4–6). The Angstrom Pyrheliometer, on the other hand, has a flat detecting element and suffers from the full ±2% uncertainty.

The uncertainty of present state-of-the-art measurements of the (infrared) surface emittance for materials such as Parsons black lacquer and other "blackening" agents is ±1 to ±2% (Refs. 8, 9, 12, 13, 14, and 15 and footnote[7]) in a carefully controlled experiment involving a particular sample. The radiative surface properties of such substances applied on a routine basis to radiometer sensors without individual determinations of absorptance must, therefore, be less well defined. Additionally, surfaces are known to change properties when exposed to high-intensity radiation environments such as that provided by the sun, or when heated to high temperatures. Furthermore, the experimental determination of infrared emittance is the only emittance measurement that can be made with as little as ±1 to ±2% uncertainty. The properties of a surface for wavelength distributions other than those of the emittance test must be established through the relative spectral response[8] of the surface in the infrared of the emittance test and in the wavelength region of interest. Such determinations of relative spectral response can be a source of additional uncertainty.

The ±1 to ±2% figures may well represent lower limits in the uncertainty of the radiative surface properties of "blackening" agents. It is clear, however, that with respect to any given uncertainty in surface absorptance, the Active Cavity Radiometer and the Active Cavity Radiometric Scale will be more accurate than the Angstrom Pyrheliometer and the International Pyrheliometric Scale. For this principal source of systematic error, the Active Cavity Radiometric scale will contain only ⅐ of the uncertainty of the International Pyrheliometric Scale.

The Active Cavity Radiometer operates in the standard detector mode at all times. Every radiation measurement is a direct determination of irradiance on the Active Cavity Radiometric Scale. As has been shown, the Active Cavity Radiometric Scale is uncertain by ±0.4% relative to the fundamental Thermodynamic Radiation Scale.

The Eppley-Angstrom Pyrheliometers used in the Table Mountain comparison tests were operated as secondary, or transfer standards (Ref. 10), their calibration constants having been determined experimentally by comparison with the standard (Stockholm) Angstrom Pyrheliometers. The fundamental uncertainty of the radiometric scale defined by an Angstrom Pyrheliometer, operated as a standard detector, with the parametric uncertainties specified in Section III, is ±2.6%. It might well be argued that an Angstrom Pyrheliometer could be constructed with a more precisely matched pair of manganin sensors than those of the Eppley-Angstrom Pyrheliometer No. 8420 and that the ±0.7% uncertainty in "compensation" current measurements would then be reduced. It should be remembered, however, that other, possibly significant sources of uncertainty have been neglected in the derivation of the ±2.6% figure (see Section III-B-3).

V. Table Mountain Comparisons of the Active Cavity Radiometric Scale and International Pyrheliometric Scale

Two experimental intercomparisons have been made of the radiometric scales defined by the Active Cavity Radiometer and the Angstrom Pyrheliometer. The basis for the experiment was a synchronous comparison of solar irradiance measurements made by the Active Cavity Radiometers and the Angstrom Pyrheliometers. The tests were conducted at the JPL Solar test site, Table Mountain Observatory. The Observatory is situated in the Angeles

[6] i.e., based upon the analysis applied to the Eppley-Angstrom Pyrheliometer No. 8420.

[7] Private communication between Plamondon, J. A., and the author of this report.

[8] The effective absorptance for the solar spectrum transmitted through 1 air mass is 0.98 ±0.02 for a freshly applied coating of Parsons black lacquer (Refs. 8–10). The effective absorptance for an infrared grey body spectral distribution corresponding to a temperature of 400°K is approximately 0.95 ±0.02+ (Ref. 9).

National Forest, 60 mi southeast of Pasadena, Calif. The elevation of the test site is 2.25 km. The geographical coordinates of the test site are 34.4°N Latitude, 117.7°W Longitude.

The first comparison experiment was conducted during May, 1968. Two Active Cavity Radiometers and two Eppley-Angstrom Pyrheliometers were operated in close proximity. Active Cavity Radiometers Nos. 1 and 5 were operated by R. Willson, D. Hoff, and C. Blankenzee. Active Cavity Radiometer No. 1 is shown in Figs. 4 and 5. The Eppley-Angstrom Pyrheliometers were Nos. 8420 and 9000. The Eppley-Angstrom test setup is shown in Fig. 6. Throughout the May experiment, Dr. Andrew Drummond of the Eppley Laboratory operated the Eppley instruments. The second intercomparison of the Active Cavity Radiometric and International Pyrheliometric scales took place during September, 1968. A representative of the Eppley Laboratory operated the Eppley-Angstrom Pyrheliometer No. 9000. Two Active Cavity Radiometers, Nos. 2 and 4, were operated. The Active Cavity Radiometer instrumentation for the second Table Mountain test is shown in Figs. 7, 8, and 9.

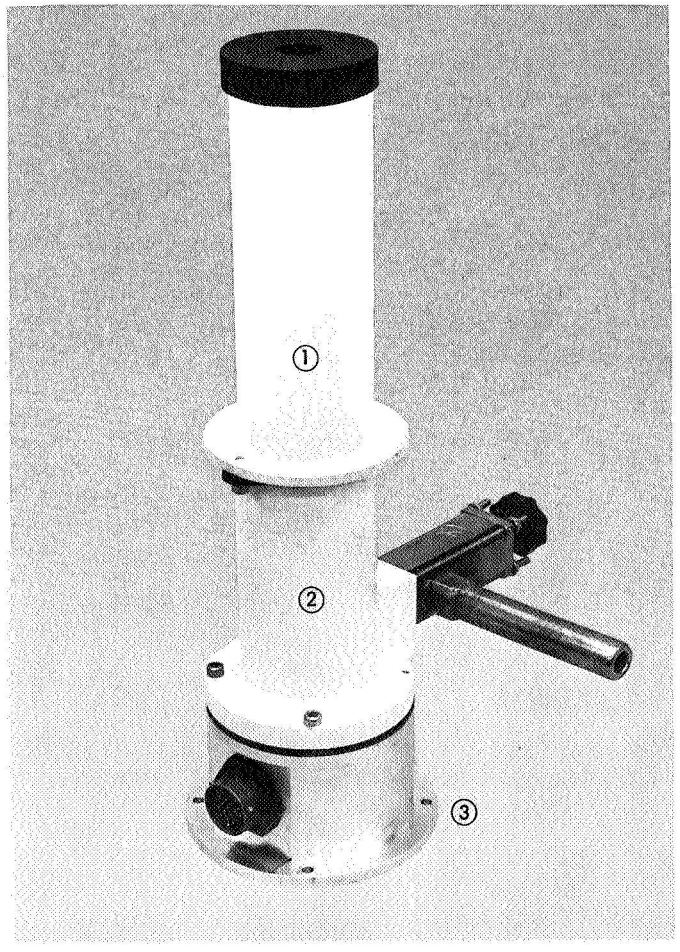

① VIEW-LIMITING ASSEMBLY

② VACUUM ENCLOSURE CONTAINING THE RADIOMETER SENSOR

③ BASE PLATE AND STANDOFF

Fig. 4. Active Cavity Radiometer No. 1

Instrumental field of view is an important factor in the intercomparison of these two types of radiometers. The Active Cavity Radiometer has a circular detector geometry and is best used with a circular field of view. The Angstrom Pyrheliometer has a rectangular detecting surface and a rectangular field of view. According to the Eppley Laboratory, the rectangular field of view of the Angstrom Pyrheliometer is equivalent to a 5-deg (full-angle) circular field of view. This equivalence will only be valid under advantageous circumstances for ground-based, solar observations (i.e., in transparent sky with a low aerosol content). Several circular apertures providing fields of view ranging from 5 to 10 deg were tried with the Active Cavity Radiometers to evaluate the experimental sensitivity to this parameter. On the days during which the data were taken, the differences observed between measurements made within this range did not exceed the experimental error. Circumsolar irradiance for fields of view less than 5 deg would be nearly equally included by both instruments, since the Angstrom field of view was 4.2 × 10.6 deg, and the field of view of the Active Cavity Radiometers was 5 deg for all of the data utilized in the comparisons.

During the May tests Dr. Drummond operated two Angstroms, making a total of 16 compensation measurements (8 per instrument) during a 20-min observing period. At the end, an average value of solar irradiance was put forth for the entire period. During the September tests, averages for shorter periods were generated (3 to 5 min).

The Active Cavity Radiometers are continuously operated in the compensation mode. Compensation for a change in irradiance is initiated automatically by a high-gain, solid-state electronic servo system. The present system is capable of providing 2400 digital data points in a 20-min period, a continuous analog record, or both. During these tests, sample data points were taken at intervals ranging from 5 s to 2 min.

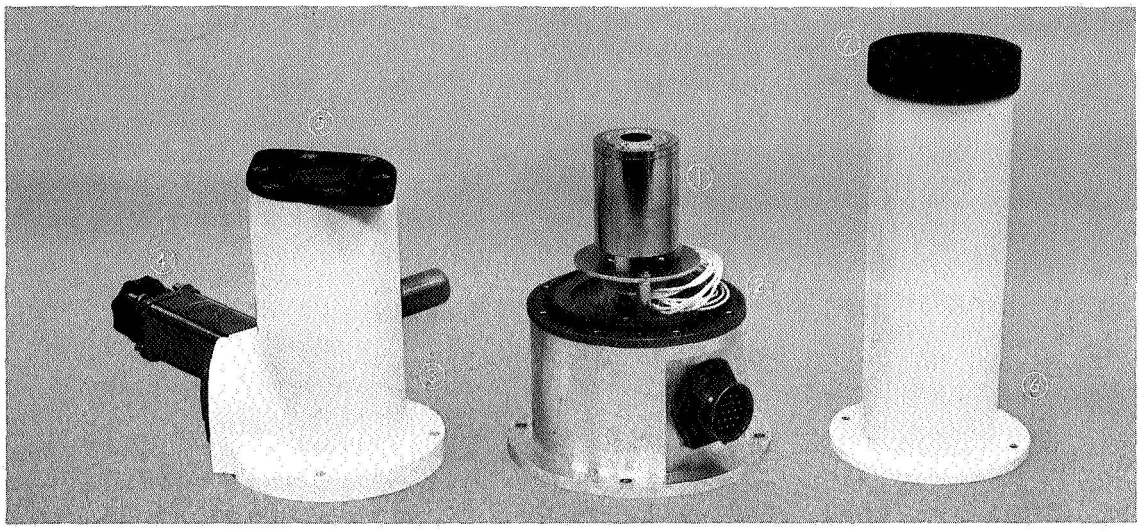

① ACTIVE CAVITY RADIOMETER No. 1

② BASE PLATE FOR RADIOMETER AND VACUUM ENCLOSURE

③ RADIOMETER VACUUM ENCLOSURE

④ VACUUM VALVE

⑤ QUARTZ WINDOW

⑥ VIEW-LIMITING ASSEMBLY

⑦ INTERCHANGEABLE VIEW-LIMITING CAP

Fig. 5. Major subassemblies of the enclosed Active Cavity Radiometer No. 1

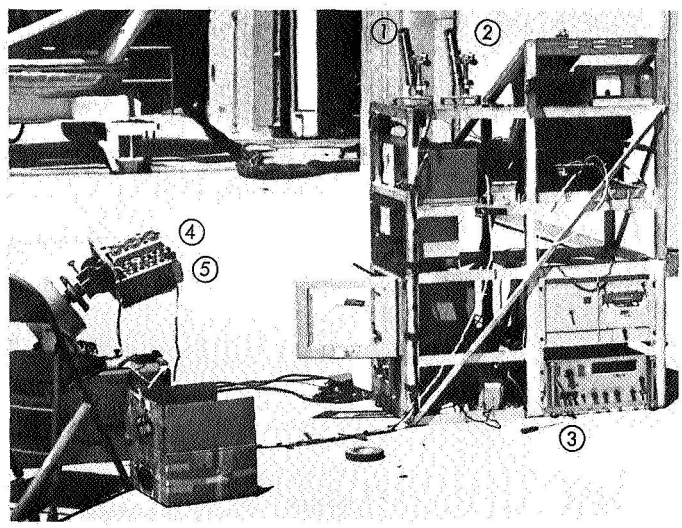

① ② EPPLEY-ANGSTROM PYRHELIOMETERS

③ EQUIPMENT RACK FOR THE ANGSTROMS AND FOR THE EPPLEY MULTICHANNEL RADIOMETERS

④ ⑤ EPPLEY MULTICHANNEL RADIOMETERS DEVELOPED BY THE EPPLEY LABORATORY FOR THE X-15 AIRCRAFT SOLAR MEASUREMENT PROGRAM

Fig. 6. Test setup for the Eppley-Angstrom Pyrheliometers Nos. 8420 and 9000 (first Table Mountain comparison test)

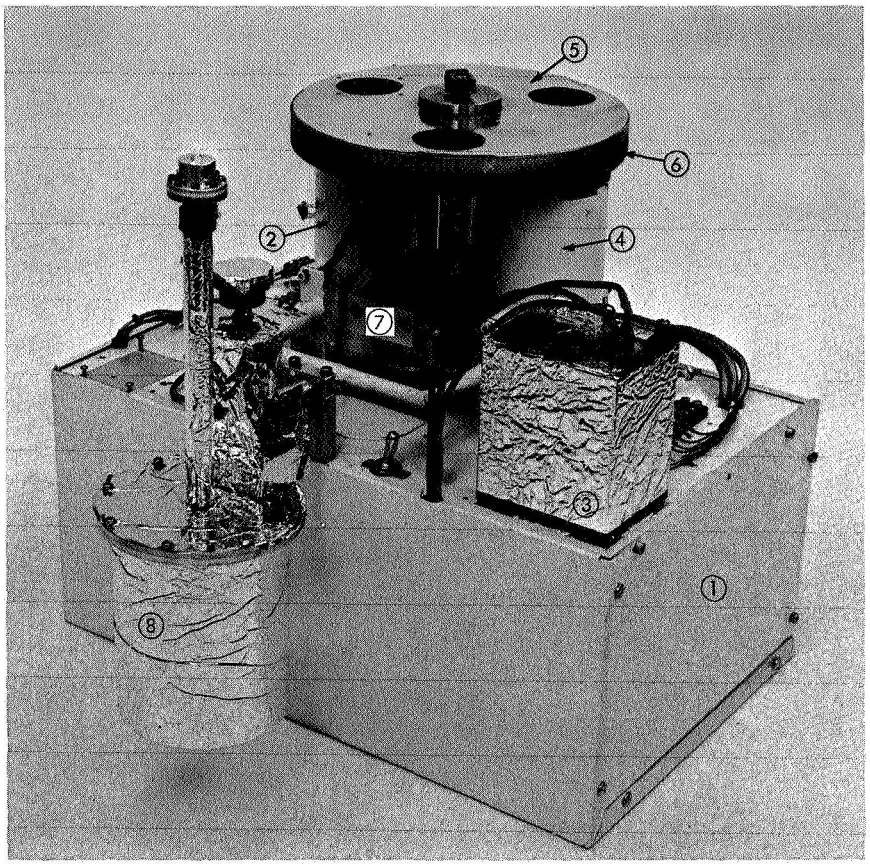

① BASE PLATE AND PROTECTIVE BOX ENCLOSING THE RADIOMETER ELECTRONIC CIRCUITRY

②④ VACUUM ENCLOSURES IN WHICH ACTIVE CAVITY RADIOMETERS Nos. 2 AND 4 ARE LOCATED

③ POWER SUPPLY (dc – dc CONVERTER)

⑤ CHOPPER WHEEL

⑥ FILTER WHEEL

⑦ TWIN GENEVA MECHANISMS FOR OPERATION OF CHOPPER AND FILTER WHEELS

⑧ CRYOGENIC VACUUM PUMP

Fig. 7. Active Cavity Radiometers Nos. 2 and 4 in the balloon-*flight configuration*. This instrumentation was used to measure the solar and spectral distribution in a high-altitude balloon experiment in August 1968, Ref. 20, and, with the addition of a 5-deg view limiter, was the Active Cavity Radiometer instrumentation used in the second Table Mountain comparison test.

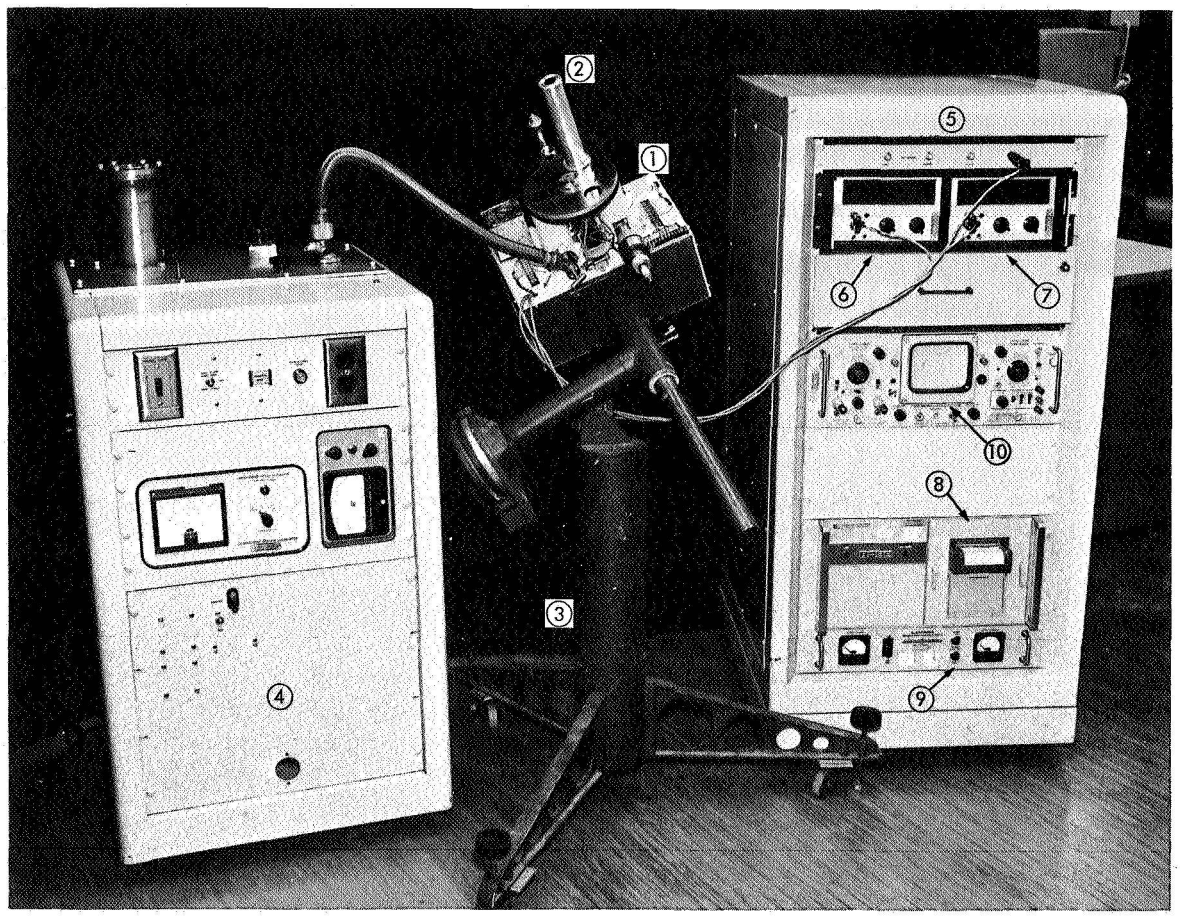

① ACTIVE CAVITY RADIOMETERS Nos. 2 AND 4 IN THE BALLOON-FLIGHT CONFIGURATION

② VIEW-LIMITING ASSEMBLY (5 deg) FOR INTERCOMPARISON WITH THE ANGSTROM PYRHELIOMETER

③ SOLAR TRACKER

④ AUXILIARY VACUUM PUMPING AND MONITORING SYSTEM. (USED ONLY DURING INITIAL EVACUATION OF THE ACTIVE CAVITY RADIOMETER ENCLOSURES)

⑤ DATA ACQUISITION AND RADIOMETER ELECTRONIC SERVICE RACKS

⑥⑦ FAIRCHILD MODEL 7000 DIGITAL VOLTMETERS. EACH OF THESE VOLTMETERS MONITORED ONE ACTIVE CAVITY RADIOMETER AND PROVIDED A VISUAL DISPLAY OF THE PRIMARY DATA (VOLTAGE V_o)

⑧ HEWLET-PACKARD MODEL 5050 A, TWO-CHANNEL DIGITAL RECORDER. THE PRIMARY DATA FROM THE FAIRCHILD DIGITAL VOLTMETERS IS PRINTED TWICE A SECOND, PROVIDING PERMANENT DATA RECORD

⑨ DC POWER SUPPLY FOR THE RADIOMETERS

⑩ TEKTRONIX RM 561 OSCILLOSCOPE USED ONLY FOR CHECKOUT OR FOR SERVICING OF RADIOMETER ELECTRONICS

Fig. 8. Active Cavity Radiometer instrumentation for Table Mountain test No. 2

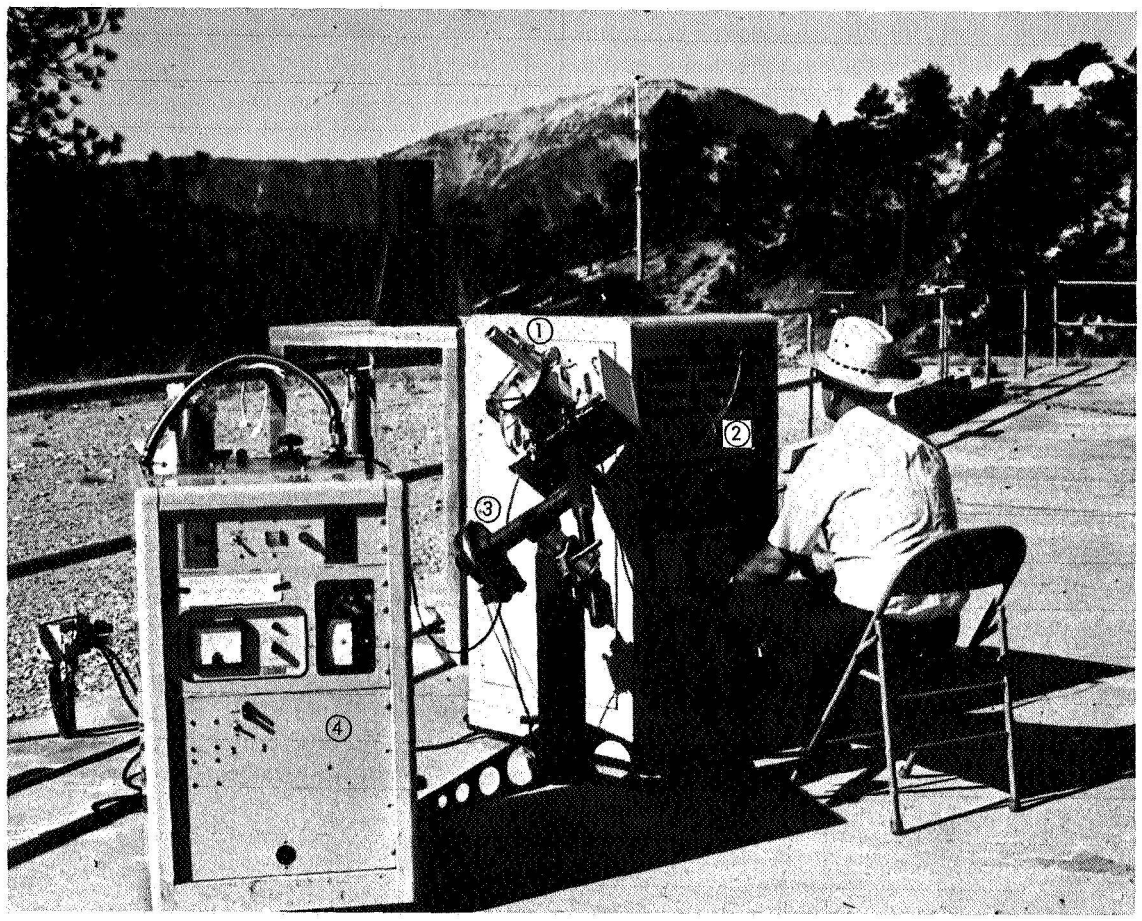

① ACTIVE CAVITY RADIOMETERS Nos. 2 AND 4 IN BALLOON-FLIGHT CONFIGURATION

② ELECTRONICS RACK CONTAINING THE DIGITAL VOLTMETERS AND PRINTER, FOR PRIMARY DATA ACQUISITION FROM THE ACTIVE CAVITY RADIOMETERS, ALONG WITH AUXILIARY ELECTRONIC EQUIPMENT

③ SOLAR TRACKER

④ AUXILIARY VACUUM RACK FOR INITIAL EVACUATION OF ENCLOSED ACTIVE CAVITY RADIOMETERS

Fig. 9. Active Cavity Radiometer instrumentation at the Table Mountain radiometer comparison test site

VI. Results of the Table Mountain Comparison Test

There were nine, 20-min observation periods during the two days of the first comparison test. In the data supplied to JPL by Dr. Drummond, there were sixteen individual measurements of solar irradiance during each 20-min period[9], eight each for the Angstrom Pyrheliometers No. 8420 and 9000. The Angstrom Pyrheliometer No. 8420 is a primary transfer standard, calibrated relative to the Stockholm Angstroms. The Angstrom Pyrheliometer No. 9000 is a secondary transfer standard, calibrated relative to the Angstrom Pyrheliometer No. 8420.

All the Active Cavity Radiometers are primary standard detectors for the Active Cavity Radiometric Scale. Agreement between the measurements made by different Active Cavity Radiometers was well within the projected experimental error. A complete set of data was gathered only with Active Cavity Radiometer No. 1 during the May test.

The first Table Mountain Comparison test is summarized in Table 1. The table presents the results obtained by the Eppley-Angstrom Pyrheliometer No. 8420 and the Active Cavity Radiometer No. 1. The solar irradiances in Table 1 are average values for 20-min observing periods.

The second Table Mountain Comparison test is summarized in Table 2. This table presents the results obtained by the Eppley-Angstrom Pyrheliometer No. 9000 and the Active Cavity Radiometer No. 2. The solar irradiances in Table 2 are average values for 3- to 5-min observing periods. Active Cavity Radiometer No. 4 was used to check the performance of Active Cavity Radiometer No. 2.

In Tables 1 and 2, the percent relative difference is defined as

$$RD = \left[1 - \frac{H_{ang}}{H_{acr}}\right] \times 10^2 \tag{93}$$

The average value of the percent relative difference for the first test was

$$\overline{RD}_1 = +2.1\% \tag{94}$$

[9]The single exception was period No. 6, a 10-min period, in which a total of eight data points was taken.

Table 1. Table Mountain comparison test No. 1[a]

Date of observation	Period of observation	Time, PDT	Angstrom Pyrheliometer No. 8420 Average Irradiance, mW/cm²	Active Cavity Radiometer No. 1 Average Irradiance, mW/cm²	Percent relative difference[b]
5/10/68	1	$\phi945$–$1\phi\phi5$	96.7	99.0	+2.3
	2	$1\phi2\phi$–$1\phi4\phi$	98.2	100.1	+1.9
	3	$11\phi\phi$–112ϕ	99.4	101.5	+2.1
	4	114ϕ–$12\phi\phi$	98.5	99.9	+1.4
	5	122ϕ–124ϕ	96.9	99.1	+2.2
	6	$13\phi5$–1315	95.2	97.1	+2.0
5/11/68	7	$\phi935$–$\phi955$	95.6	98.0	+2.4
	8	$1\phi2\phi$–$1\phi4\phi$	98.0	100.6	+2.6
	9	111ϕ–113ϕ	98.6	100.9	+2.3

[a]This is a comparison of the average solar irradiances measured over 20-min periods by the Eppley-Angstrom Pyrheliometer and the JPL Active Cavity Radiometer on May 10 and 11, 1968 at Table Mountain, Calif.
[b]$\overline{RD}_1 = +2.1\%$ (average value of the percent relative difference).
$S(\overline{RD}_1) = \pm 0.12\%$ (standard deviation of the average value of the percent relative difference).

The standard deviation of the average value of the percent relative difference is based upon an error function for a Gaussian residual distribution. For n observations, the standard deviation of $\overline{RD}$ is

$$S(\overline{RD}) = \pm \left[\frac{\Sigma_i \Delta_i^2}{n(n-1)}\right]^{1/2} \tag{95}$$

where Δ_i^2 is the square of the i^{th} residual.

The standard deviation of the average value of the percent relative difference was

$$S(\overline{RD}_1) = \pm 0.12\% \tag{96}$$

The 20-min averages reported in Table 1 are the result of averaging over eight readings in the case of the Angstrom data. The number of data points used in finding the Active Cavity Radiometer averages varied throughout the test, ranging from 10 to 153. The time averages for the Active Cavity Radiometer were computed using the relationship

$$H_{ACR} = \frac{\Sigma_i (1/2)(H_i + H_{i+1})(t_{i+1} - t_i)}{\sum_i (t_{i+1} - t_i)} \tag{97}$$

Table 2. Table Mountain comparison test No. 2[a]

Date of observation	Observation period	Time, PDT	Angstrom Pyrheliometer No. 9000 average irradiance, mW/cm²	Active Cavity Radiometer No. 2 average irradiance, mW/cm²	Percent relative difference[b]	Date of observation	Observation period	Time, PDT	Angstrom Pyrheliometer No. 9000 average irradiance, mW/cm²	Active Cavity Radiometer No. 2 average irradiance, mW/cm²	Percent relative difference[b]
9/23/68	1	1500	102.6	104.9	2.2	9/25/68					
↓	2	1515	101.4	103.7	2.2	(contd)	21	1002	100.5	102.7	2.1
↓	3	1530	101.2	103.3	2.0	↓	22	1015	101.1	103.3	2.1
9/24/68	4	1000	101.7	103.7	1.9		23	1027	101.8	104.2	2.3
↓	5	1015	102.2	104.9	2.6		24	1035	102.4	104.4	1.9
↓	6	1020	103.1	105.4	2.2		25	1105	103.4	105.3	1.8
↓	7	1030	103.5	106.1	2.4		26	1120	103.8	106.0	2.0
↓	8	1045	104.0	106.4	2.3		27	1140	104.3	106.2	1.8
↓	9	1051	104.2	107.1	2.7		28	1148	104.3	106.6	2.2
↓	10	1100	104.8	107.2	2.2		29	1157	104.3	106.4	2.0
↓	11	1105	104.8	107.2	2.2		30	1210	104.3	106.8	2.3
↓	12	1145	106.0	108.6	2.4		31	1246	104.5	106.7	2.1
↓	13	1200	106.1	108.6	2.3		32	1300	104.2	106.4	2.0
↓	14	1245	105.9	108.8	2.7		33	1315	104.3	106.3	1.9
↓	15	1300	106.1	108.4	2.1		34	1332	103.6	105.8	2.1
9/24/68	16	1422	104.3	106.9	2.4		35	1344	103.6	105.6	1.9
↓	17	1430	103.9	106.4	2.4		36	1354	102.7	105.4	2.5
↓	18	1440	102.6	105.5	2.6		37	1410	102.2	104.2	1.9
9/25/68	19	1450	102.5	104.7	2.1		38	1420	101.8	103.8	1.9
↓	20	0950	99.4	101.4	2.0	↓	39	1430	101.1	103.6	2.4

[a]This is a comparison of the average value of solar irradiances measured over 3- to 5-min periods by the Eppley-Angstrom Pyrheliometer No. 9000 and the Active Cavity Radiometer No. 2.

[b]$\overline{RD_2} = 2.2\%$ (average value of the percent relative difference).
$S(\overline{RD_2}) = \pm 0.04\%$ (standard deviation of the average value of the percent relative difference).

In this manner, the unequal time spacing of some data points was corrected for by weighting the measured irradiances by the time spacing between adjacent points.

Here

H_i = the measurement of irradiance, i^{th} data point

$(t_{i+1} - t_i)$ = the time separation of the i^{th} and the $(i + 1)^{th}$ irradiance measurement

The results of the second Table Mountain Comparison test are presented in Table 2. There were 39 intercomparisons of the Active Cavity Radiometer No. 2 and the Angstrom Pyrheliometer No. 9000 during the September test. The results supplied by the Eppley Laboratories for the Angstrom Pyrheliometer No. 9000 were average values for each of the observation periods. The irradiances shown for the Active Cavity Radiometer No. 2 are averages of 5 to 10 individual measurements made during each observation period.

The average value of the percent relative difference for the second Table Mountain test was

$$\overline{RD_2} = +2.2\% \tag{98}$$

The standard deviation of the average value of the percent relative difference is

$$S(\overline{RD}_2) = \pm 0.04\% \tag{99}$$

The resultant average value of the percent relative difference for the two Table Mountain tests may be determined by weighting the average value for each test by the total number of measurements involved in the determination of each average. An expression defining this quantity may be written as

$$RD = \frac{n_1 \overline{RD}_1 + n_2 \overline{RD}_2}{n_1 + n_2} \tag{100}$$

The resultant average value of the percent relative difference for both tests is

$$RD = +2.2\% \tag{101}$$

VII. Conclusions

The experimentally determined relative difference between the Active Cavity Radiometric Scale, as defined by the Active Cavity Radiometer, and the International Pyrheliometric Scale, as conserved by the Eppley-Angstrom Pyrheliometers Nos. 8420 and 9000 is

$$\boxed{RD = +2.2\%} \tag{102}$$

The uncertainty of the Active Cavity Radiometric Scale is equal to the uncertainty of measurements made with the Active Cavity Radiometer. As shown in Section II, this uncertainty is $\pm 0.4\%$. The relative difference between the two scales is then

$$\boxed{RD = +2.2 \pm 0.4\%} \tag{103}$$

The difference between the two radiometric scales exceeds the uncertainty of measurements on the Active Cavity Radiometric Scale, and is positive, indicating that measurements of irradiance on the International Pyrheliometric scale contain a systematic error of from -1.8% to -2.6% and are, therefore, lower than the true value on the fundamental thermodynamic radiation scale. An error of this magnitude in the International Pyrheliometric Scale falls well within the uncertainty of measurements made by the Angstrom Pyrheliometer. It may be noted that an overestimation of the detector absorptance (α in Eq. 68) will produce an underevaluation of irradiance by the Angstrom.

Measurements made on the International Pyrheliometric Scale may now be converted to the Active Cavity Radiometric Scale. The relative difference between irradiance measurements on the Active Cavity Radiometric Scale and the International Pyrheliometric Scale is defined as

$$RD = \frac{H_{\text{ACRS}} - H_{\text{IPS}}}{H_{\text{ACRS}}} \tag{104}$$

where

H_{ACRS} = irradiance measured on the Active Cavity Radiometric Scale (ACRS).

H_{IPS} = irradiance measured on the International Pyrheliometric Scale (IPS).

Solving for H_{ACRS}

$$H_{\text{ACRS}} = [1 - RD]^{-1} H_{\text{IPS}} \tag{105}$$

Evaluating $[1 - RD]^{-1}$ the conversion relationship is obtained:

$$\boxed{H_{\text{ACRS}} = 1.022\, H_{\text{IPS}}} \tag{106}$$

It is of interest to apply this relationship to the results of a recently reported solar constant measurement (Refs. 16 and 17). A radiometer designed by the Eppley Laboratory and calibrated relative to the International Pyrheliometric Scale was flown to an altitude of 82 km aboard a NASA X-15 research aircraft. Figure 6 shows the multichannel radiometers developed for that experiment. The value of the solar constant reported by Laue and Drummond for this experiment was:

$$Ho_{\text{IPS}(x\text{-}15)} = 136.1 \text{ mW/cm } (1.951 \text{ cal/cm}^2\text{/min}) \tag{107}$$

Reporting this measurement on the Active Cavity Radiometric Scale by the use of Eq. (106) gives

$$Ho_{\text{ACRS}(x\text{-}15)} = 139.1 \text{ mW/cm}^2 \ (1.995 \text{ cal/cm}^2\text{/min}) \tag{108}$$

The solar constant value commonly accepted in the U. S. from 1954 to 1965 was that proposed by F. S. Johnson (Ref. 18). His value was based on an analysis of over 30 years of ground-level solar irradiance data taken by the Smithsonian Astrophysical Observatory. The data

are reported on the radiometric scale defined by a standard detector referred to as the Abbott Silver-Disk Pyrheliometer.

$$Ho_{FSJ} = 139.5 \text{ mW/cm}^2 \text{ (2.00 cal/cm}^2\text{/min)} \quad (109)$$

where FSJ stands for F. S. Johnson.

A re-evaluation of the Smithsonian data was performed by P. R. Gast and reported in 1965 (Ref. 19). Gast incorporated into his analysis some recent solar ultraviolet data that had been gathered by rocket-borne spectrographs. The resulting solar constant value was

$$Ho_{PRG} = 139.0 \text{ mW/cm}^2 \text{ (1.992 cal/cm}^2\text{/min)} \quad (110)$$

where PRG stands for P. R. Gast.

The solar constant value determined by the X-15 aircraft experiment, when reported relative to the Active Cavity Radiometric Scale, differs by only -0.3% from the Johnson value and by less than $+0.1\%$ from the Gast value.

A high-altitude balloon experiment was performed (Ref. 20) in August, 1968 in which measurements of the solar constant and spectral distribution were made on the Active Cavity Radiometric Scale. Two Active Cavity Radiometers were operated at an altitude of 24 km for 4 h and 30 min. After correcting the measurements for the effects of the remaining atmosphere and the Earth-to-sun distance, the solar constant value was

$$\boxed{Ho_{ACRS(B)} = \begin{cases} 139.0 \pm 1 \text{ mW/cm}^2 \text{ or} \\ 1.992 \pm 0.013 \text{ cal/min/cm}^2 \end{cases}} \quad (111)$$

The uncertainty of ± 1 mW/cm^2 ($\pm 0.7\%$) exceeds the value for an equivalent ground-based measurement by an Active Cavity Radiometer. The increase in uncertainty from ± 0.4 to $\pm 0.7\%$ was introduced into the data by the telemetry uncertainty, the larger uncertainty in the transmittance of the instrument windows for the solar spectrum at 24 km, and the uncertainty of the effects of the remaining, intervening atmosphere between the radiometers and the sun.

The high-altitude balloon experiment was the first direct measurement of the solar constant by a standard detector in which the uncertainty of the atmospheric transmittance for solar radiation was not the dominant source of error. For this reason, it is felt that the value of the solar constant produced from the experiment represents the most accurate determination available at present.

References

1. Plamondon, J. A., Kendall, J. M. Sr., "A Cavity-Type, Absolute, Total-Radiation Radiometer," Space Programs Summary 37-35, Vol. IV. Jet Propulsion Laboratory, Pasadena, Calif., Sept. 13, 1965.
2. Kendall, J. M. Sr., *The JPL Standard Total-Radiation Absolute Radiometer,* Technical Report 32-1263, Jet Propulsion Laboratory, Pasadena, Calif., May 5, 1968.
3. Willson, R. C., *Radiometer Comparison Tests,* Technical Memorandum 33-371, Jet Propulsion Laboratory, Pasadena, Calif., Dec. 15, 1968.
4. Syndor, C., *An Analytical Study of Some Cavity Radiometer Properties,* Technical Report, Jet Propulsion Laboratory, Pasadena, Calif., in Press, 1968.
5. Sparrow, E. M., Jonsson, V. K., "Radiant Emission Characteristics of Diffuse Conical Cavities," *J. Opt. Soc. Am.,* Vol. 53, p. 816, 1963.
6. Sparrow, E. M., "Radiation Heat Transfer Between Surfaces," *Advan. Heat Transf.,* Vol. II, p. 400, Academic Press, 1965.

References (contd)

7. Lin, Siang-Hui, "Radiant Interchange in Cavities and Passages with Specularly and Diffusely Reflecting Surfaces," Thesis, University of Minnesota, 1964.
8. Blevin, W. R., Brown, W. J., "Black Coatings for Absolute Radiometers," *Metrologia,* 1967.
9. Stierwalt, D. L., *Infrared Spectral Emissivity of Optical Materials* NOLC Report 537, U.S. Naval Ordnance Laboratory, Corona, Calif., Jan. 1966.
10. "The Eppley-Angstrom Compensation Pyrheliometer and Associated dc Electrical Instrumentation," Instruction Manual published by the Eppley Laboratory, Inc., Newport, Rhode Island.
11. Goody, R. M., *Atmospheric Radiation,* Vol. I, p. 418, Oxford (Clarendon) Press, 1964.
12. Jacquez, J., et. al., "Integrating Sphere for the Measurement of Reflectance with the Beckman Model Dr Recording Spectrophotometer, *J. Opt. Soc. Am.,* Vol. 45, p. 971, 1955.
13. Harris, L., Cuff, K., "Reflectance of Goldblack Deposits and Some Other Materials of Low Reflectance from 254 mu to 1100 mu. The Scattering Unit Size in Goldblack Deposits," *J. Opt. Soc. Am.,* Vol. 46, p. 160, 1956.
14. Derksen, W. L., "Automatic Recording Reflectometer for Measuring Diffuse Reflectance in the Visible and Infrared Regions," *J. Opt. Soc. Am.,* Vol. 47, p. 995, 1957.
15. Brandenberg, W. M., Neu, J. T., "Unidirectional Reflectance of Imperfectly Diffuse Surfaces," *J. Opt. Soc. Am.,* Vol. 56, 1966.
16. Drummond, A. J., Laue, E. G., et. al, "Multichannel Radiometer Measurement of Solar Irradiance," *J. Spacecraft Rockets,* Vol. 4, p. 1200, Sept., 1967.
17. Drummond, A. J., Laue, E. G., *Direct Measurement from High-Altitude Aircraft of the Solar Constant of Radiation,* Report, Eppley Laboratory, Inc., Newport, Rhode Island, in press, 1968.
18. Johnson, F. S., "The Solar Constant," *J. Meterolog.,* Vol. 11, No. 6, p. 431, Dec., 1954.
19. Gast, P. R., *Handbook of Geophysics and Space Environments,* 16-1, McMillan Press, 1965.
20. Willson, R. C., *High-Altitude Measurement of the Solar Constant and Spectral Distribution,* Technical Report, Jet Propulsion Laboratory, Pasadena, Calif., in press.